Scalable ultrasmall three-dimensional nanowire transistor probes for intracellular recording

Yunlong Zhao [1,2,6], Siheng Sean You [1,6], Anqi Zhang[1,6], Jae-Hyun Lee[1,3], Jinlin Huang[1] and Charles M. Lieber [1,4,5]*

New tools for intracellular electrophysiology that push the limits of spatiotemporal resolution while reducing invasiveness could provide a deeper understanding of electrogenic cells and their networks in tissues, and push progress towards human–machine interfaces. Although significant advances have been made in developing nanodevices for intracellular probes, current approaches exhibit a trade-off between device scalability and recording amplitude. We address this challenge by combining deterministic shape-controlled nanowire transfer with spatially defined semiconductor-to-metal transformation to realize scalable nanowire field-effect transistor probe arrays with controllable tip geometry and sensor size, which enable recording of up to 100 mV intracellular action potentials from primary neurons. Systematic studies on neurons and cardiomyocytes show that controlling device curvature and sensor size is critical for achieving high-amplitude intracellular recordings. In addition, this device design allows for multiplexed recording from single cells and cell networks and could enable future investigations of dynamics in the brain and other tissues.

D eveloping new tools that enable reproducible high spatial–temporal resolution recording of intracellular potential, while maintaining the capability for device scalability, are key goals for advancing electrophysiology studies of electrogenic cells and cell networks[1–4]. Patch-clamp electrodes have been the gold standard for cell electrophysiology for decades, and they have shown that accurate recording of the intracellular potential requires a high-resistance seal against the cell membrane and low resistance between the recording element and the cell interior[5,6]. Recent studies have focused on several solid-state nanodevice architectures, including nanowire-based structures for optical neuronal stimulation[7,8], scalable on-chip micro/nano-structured electrode arrays[9,10] for attenuated intracellular recording via electroporation[11,12] and/or optoporation[13,14], and three-dimensional (3D) nanowire field-effect transistor probes for intracellular recording of single cells[15,16]. Nanowire probes have recorded cardiac intracellular action potentials with amplitudes comparable to those recorded with patch-clamp micropipettes[15,16], but have relied on one-by-one fabrication that has been difficult to scale up. For solid-state nanoprobes to achieve comparable recording signal-to-noise ratio and amplitude to those of patch clamp measurements, the nanodevice must achieve direct contact of the recording element with the intracellular solution without significantly disturbing the cell membrane[2,9]. Fulfilling these criteria requires understanding the size, geometry and mechanical and biochemical factors present at the cell membrane–nanodevice interface. Recent work suggests that nanoscale size and geometry play a key role in the interaction between the nanostructure and the cell membrane[17,18]. For example, nanoscale membrane curvature elevates the local concentration of endocytosis-related proteins[17,18], influences the conformation and activity of transmembrane proteins[19] and is hypothesized to recruit a sequence of proteins leading to membrane fission[20]. Building on these studies, we hypothesize that inducing appropriate nanoscale curvature

on the cell membrane via rational device design will facilitate probe internalization and enable intracellular recording.

Here, we investigate how the size and geometry of nanoprobes influence intracellular recording by fabricating scalable 3D U-shaped nanowire field-effect transistor (U-NWFET) arrays in which both the radii of curvature (ROC) and active sensor sizes are controlled (Fig. 1a). To investigate how these design factors affect electrophysiological recording, arrays of U-NWFET probes fabricated from 15-nm-diameter p-type Si nanowires with ROC from 0.75 to 2 μm and active channel lengths from 50 to 2,000 nm were used to probe cultured primary neurons and human cardiomyocytes. Schematically, we ask whether probes with the smallest ROC and sensor size (Fig. 1b(i)) can facilitate recording full amplitude intracellular action potentials and subthreshold features, where increases in the ROC and detector sizes (Fig. 1b(ii)) would lead to recording smaller amplitude intracellular-like or extracellular action potential peaks.

U-shaped nanowire probe fabrication and characterization

Our strategy for producing reproducible arrays of U-NWFET probes with controlled ROC and active FET channel lengths or detector sizes involves two key techniques (see Methods for details). First, large-scale, shape-controlled deterministic assembly[21] is used to produce U-shaped nanowire arrays from 15-nm-diameter Si nanowires with controllable ROC on top of Si_3N_4 patterns (Fig. 2a(i) and Supplementary Fig. 1a–e). Metal contacts are then deposited and passivated by an upper Si_3N_4 layer (Supplementary Fig. 1f). Second, we exploit spatially defined solid-state transformation[22] to convert Si nanowire segments underneath and adjacent to the Ni diffusion layer to metallic NiSi, thereby producing a controlled length of FET sensing elements at the tips of the U-shaped nanowire probes (Fig. 2a(ii) and Supplementary Fig. 1g). Finally, etching of the sacrificial layer allows the probes to bend upward
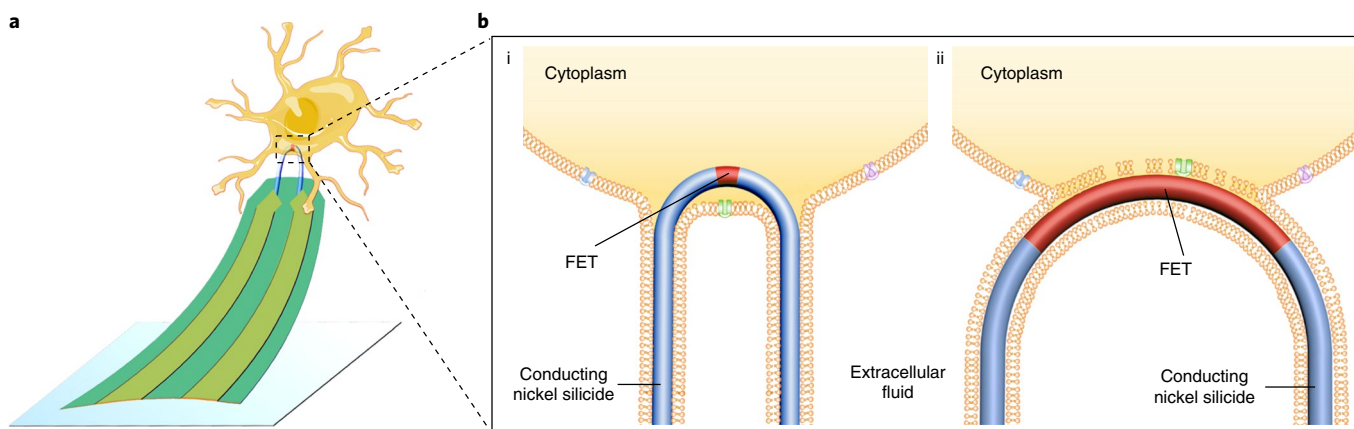
Fig. 1 | Ultrasmall U-NWFET probe as a new approach for electrophysiology. a, Schematics of intracellular recording by a U-NWFET probe. The location, size, geometry of each probe and the sensor size can be well modulated by a deterministic shape-controlled nanowire transfer technique and spatially defined transformation of Si nanowire segments to NiSi, respectively. **b**, Schematics of two possible probe–cell interfaces. (i) Internalization and high-resistance seal of a short-channel U-NWFET to the cell membrane enables high-amplitude recording. The sensitive p-type Si NWFET region and the metallic NiSi region on the U-shaped nanowire are marked with red and blue-grey, respectively. The nanowire is shown modified with phospholipid. (ii) Partial sealing/internalization of the U-NWFET with longer channel length/ROC results in attenuated intracellular-like action potential recording.

due to interfacial strain in the metal interconnects (Fig. 2a(iii))[15], yielding probe arrays with up to four addressable U-NWFETs per bend-up probe arm (Supplementary Fig. 1h).

Optical microscopy and scanning electron microscopy (SEM) were used to characterize key steps in the U-NWFET probe fabrication flow. Optical microscopy images of the patterned bottom passivation layer and U-shaped trenches that set the ROC during nanowire assembly (Supplementary Fig. 2a,b) as well as three probes with U-shaped nanowires, metal contacts and top passivation layer (Fig. 2b) are indicative of the deterministic parallel assembly of U-shaped nanowire probes with defined ROC. Composition-sensitive SEM images of U-NWFETs following annealing of the patterned Ni further highlight the control of channel lengths from ~50 nm (Fig. 2c) to 500 and 2,000 nm (Supplementary Fig. 2c,d). Measured channel lengths and ROCs were found to be consistent with those designed (Supplementary Fig. 3). Etching of the Ni release layer produces arrays of probes, including single U-NWFET probes (Fig. 2d) and multiple U-NWFET devices on a single probe arm (Supplementary Fig. 2e) where the active U-NWFET sensor elements are oriented upwards away from the substrate.

Electrical transport studies in air and aqueous solution were carried out to characterize the sensor properties. Current versus drain–source voltage (I–V_{ds}) measurements on devices with channel lengths of ~50, 500 and 2,000 nm (Fig. 2e–g; $N = 10$, each channel length) in the dry state yield average conductances of 3.3 ± 0.6, 0.7 ± 0.2 and $0.3 \pm 0.1\,\mu$S, respectively. In addition, conductance versus water gate voltage (V_g) measurements in aqueous solution (Fig. 2h–j) yield average transconductances of 5.4 ± 1.3, 2.3 ± 0.7 and $0.9 \pm 0.3\,\mu$S V^{-1} for 50, 500 and 2,000 nm channel lengths, respectively. Plots of probe transconductance versus ROC (0.75–2.0 μm) for devices with 50, 500 or 2,000 nm FET channels (Supplementary Fig. 4 and Supplementary Table 1) show that transconductance does not significantly vary as a function of ROC in our designed strain range (Supplementary Table 2). The conductance and transconductance results for the U-NWFETs are roughly consistent with the expected inverse relationship to the channel length. Finally, the transconductance and measured noise values yield an estimate for signal detection sensitivity (three standard deviations) of 0.90 ± 0.60, 1.2 ± 0.9 and 1.9 ± 0.9 mV for 50, 500 and 2,000 nm channel lengths, respectively, which should allow detection of the typical 1–10 mV subthreshold activities of neurons[2].

Near full amplitude intracellular recordings

With these characterization results, we first asked whether ultrasmall U-NWFET probes could record full amplitude intracellular action potentials from primary neurons. First, a single U-NWFET probe with ~50 nm FET length and 0.75 μm ROC was used to sequentially measure six independent dorsal root ganglion (DRG) neurons (see Methods and Supplementary Fig. 5), where the probe was not remodified with lipid between the sequential measurements (Supplementary Fig. 6). In each trace, we observe a drop in the baseline potential upon initial cell contact (Fig. 3a). Subsequently, either sparse peaks (cells 1, 3 and 6) or periodic peaks (cells 2, 4 and 5) are observed with amplitude of 60–100 mV and signal-to-noise ratios of 115 ± 29. For each cell, the recorded potentials have consistent shape and duration, and characteristic single peaks recorded from the six cells are shown in Fig. 3b. An additional set of data recorded from two DRG neurons without spontaneous firing properties showed a voltage drop (Supplementary Fig. 7a), or one single peak followed by a voltage drop (Supplementary Fig. 7b), during device penetration. Following the initial recording, we observed a gradual decrease in the peak amplitude as well as a positive shift in the baseline potential (Fig. 3c,d and Supplementary Fig. 7).

These recordings highlight several key features. First, the waveforms, amplitudes, firing patterns and signal-to-noise ratios of the peaks are similar to our patch-clamp recordings of similarly cultured DRG neurons (Supplementary Fig. 8) and are consistent with the reported heterogeneity of spontaneously firing DRG action potential waveforms and spike patterns[23]. These data thus indicate that the ultrasmall U-NWFETs with biomimetic phospholipid modification can provide high-resistance membrane seals, achieve direct access to the cell interior, and yield faithful recording of the intracellular potential. Notably, the data recorded from some DRG neurons exhibit characteristics consistent with mechanosensitive properties[24], including an increase in action potential firing rate (Fig. 3c,d) and firing of a single action potential (Supplementary Fig. 7b) during formation of the device/cell junction. A limitation of the recording is, however, the shift in baseline and decrease in recorded action potential amplitude at later times (for example, Fig. 3c). We suggest that these changes are due to either an elastic response from the cytoskeleton, which gradually pushes the probe out of the cell as suggested in other intracellular chemical delivery experiments[25], or mechanical instability of the measurement set-up.
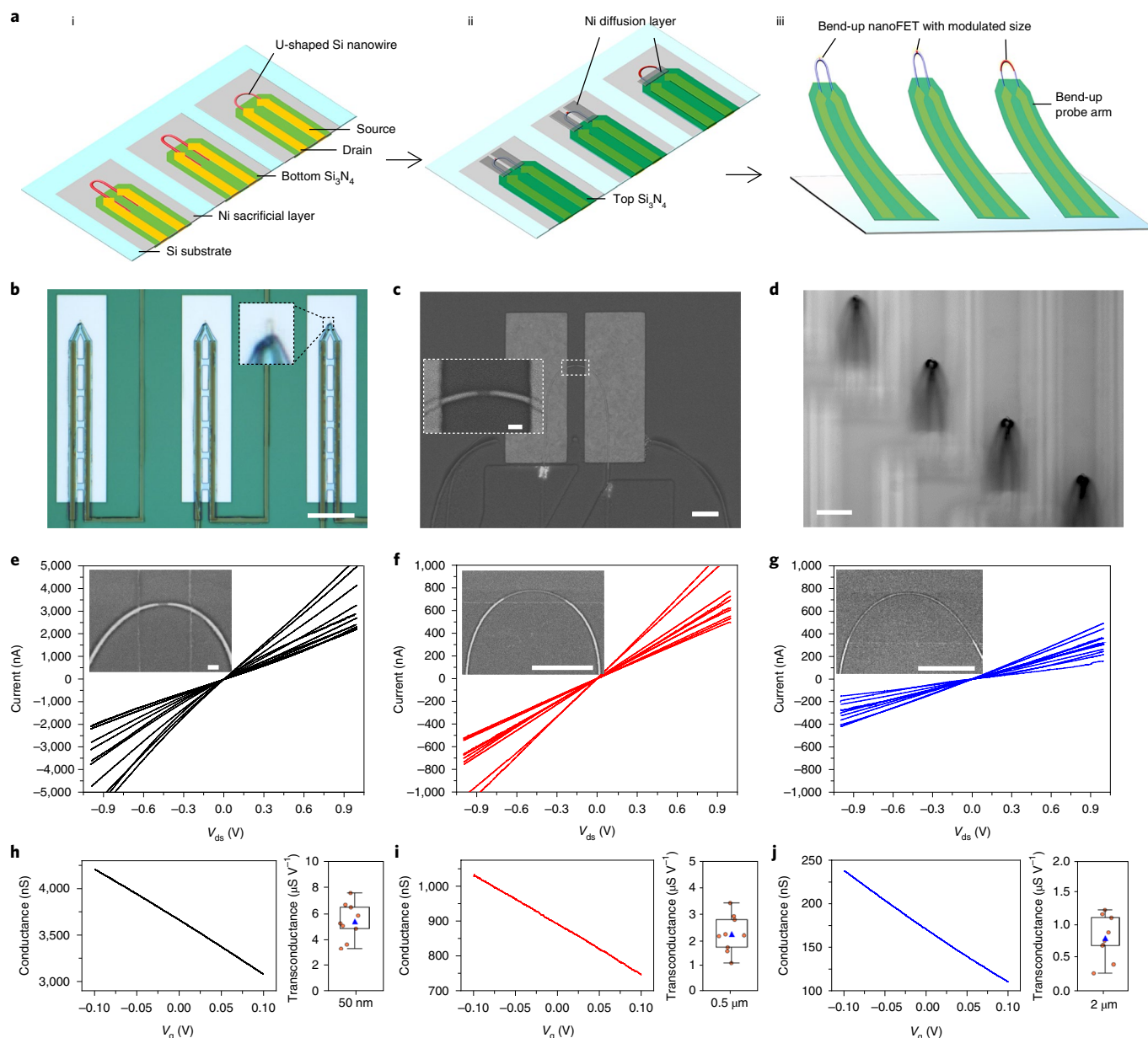
Fig. 2 | Fabrication and characterization of U-NWFET probes. a, Schematics of device fabrication. (i) Assembly of U-shaped nanowire devices on a Ni sacrificial layer and bottom Si_3N_4 passivation layer; electrical contacts to the transferred U-shaped nanowires are made via deposition of Cr/Au/Cr (1.5/60/60 nm) metal interconnects, where the relative Cr/Au/Cr thicknesses yield a built-in strain that bends the probe up upon release. (ii) Deposition of the top Si_3N_4 passivation layer and the Ni diffusion layer followed by rapid thermal annealing to transform the Si nanowire segments underneath and adjacent to the Ni diffusion layer to NiSi, thus generating a local FET at the tip of the U-shaped nanowire. (iii) Probes bending upward after etching the Ni diffusion and sacrificial layers. **b**, Optical image of three devices following deposition of metal interconnects and before deposition of the nickel diffusion layer. Inset, magnified view showing that a U-shaped nanowire is deterministically transferred to the device tip. Scale bar, 20 µm. **c**, SEM image of the device after Ni diffusion. Scale bar, 500 nm. Inset, magnified SEM image of the dashed region showing the resulting local FET at the U-shaped nanowire tip. Imaging with backscattered electrons (BSE) shows the Si (dark region) and NiSi (bright region) distribution on the U-shaped nanowire. Scale bar, 50 nm. **d**, Optical image of the bend-up device array in water. Scale bar, 20 µm. **e–g**, Current versus drain–source voltage (V_{ds}) traces for 10 devices in the dry state for ~50 nm (**e**), ~500 nm (**f**) and ~2,000 nm (**g**) channel lengths. Insets, SEM images taken using the BSE mode of the local FET following removal of the Ni layer. Scale bars, 50 nm (**e**), 0.5 µm (**f**), 0.5 µm (**g**). **h–j**, Left, conductance versus reference water gate potential (V_g) recorded from one representative device for each channel length (~50 nm (**h**), ~500 nm (**i**) and ~2,000 nm (**j**)) in Tyrode's solution. Right, box and whisker plots showing the distribution ($N = 10$) of transconductance for devices of each channel length gated by a reference electrode in Tyrode's solution. The blue triangle shows the mean of the transconductances, the top and bottom edges of the box indicate the upper/lower quartiles and the whiskers indicate the highest and lowest measured values, respectively.

Given the high signal-to-noise ratio for our measurements, we asked whether it was possible to observe subthreshold activity. Notably, close examination of a representative trace from a cell

with irregular firing pattern (Fig. 3d) shows subthreshold features, including a single ~5 mV peak (Fig. 3e(i)) and a series of three small peaks (Fig. 3e(iii)) immediately before the initiation of an action
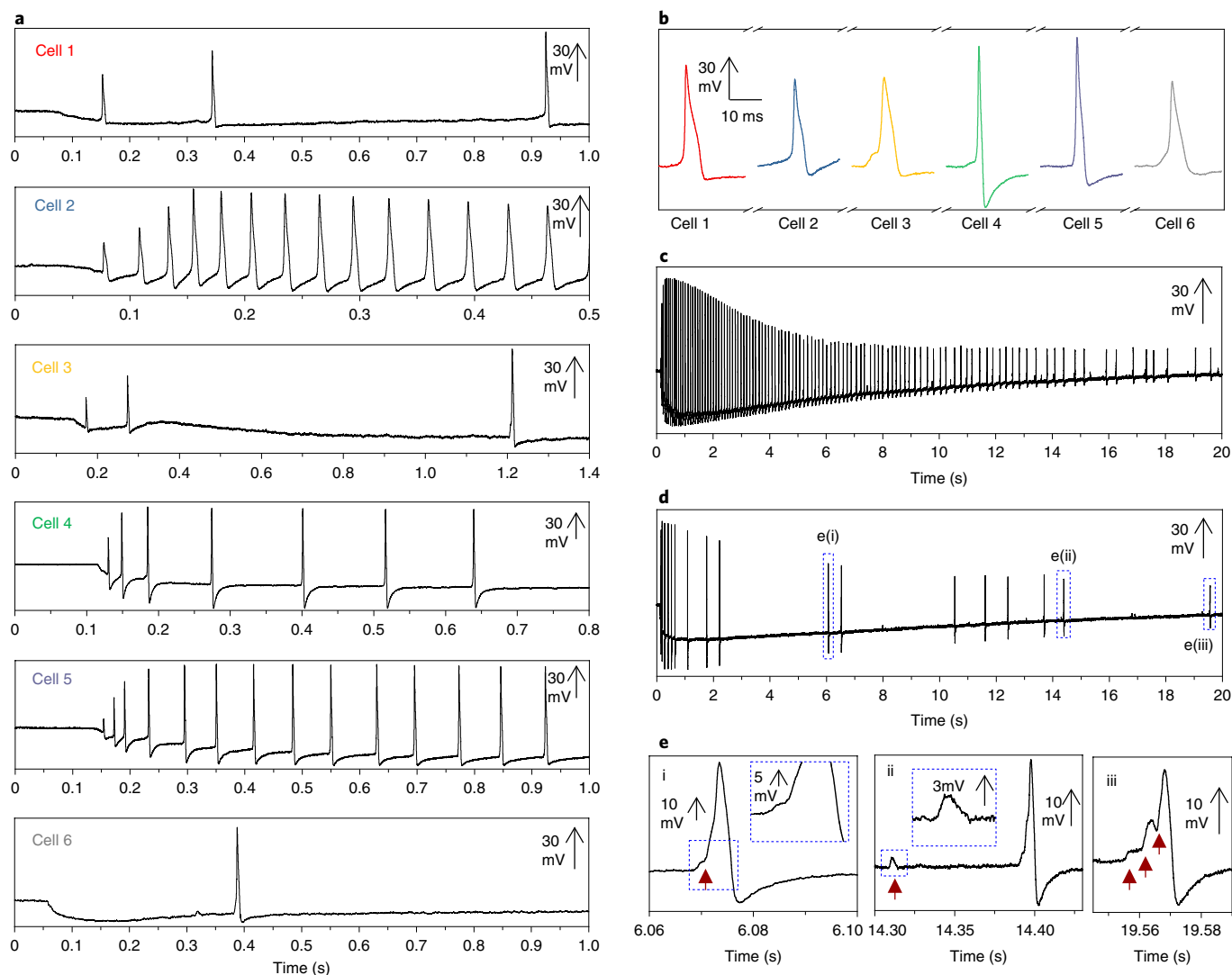
Fig. 3 | Intracellular recording of DRG neurons by the ultrasmall U-NWFET probe. a, Intracellular action potentials recorded sequentially from six independent neurons using the same U-NWFET probe without remodification. The numbering of the cells indicates the order in which the measurements occurred. The probe has a FET channel length of ~50 nm and ROC of 0.75 μm. **b**, Summary of recorded action potentials from the six different cells in **a** in chronological order. The maximum signal amplitude remains similar between these measurements, showing that the probe is highly reusable. The signal-to-noise ratio of these recordings is 115 ± 29 ($N = 6$). **c**, Intracellular recording trace from a cell with regular firing pattern showing a gradual increase in baseline potential and decrease in action potential amplitude. **d**, Representative trace from a cell with irregular firing pattern; subthreshold activities appear in regions outlined by blue dashed lines. **e**, Enlarged regions of three different areas from **d** showing different types of subthreshold activity, highlighted by the red arrows and blue dashed regions.

potential, as well as an ~3 mV peak not associated with an action potential spike (Fig. 3e(ii)); we recorded similar results with patch-clamp (blue triangles, Supplementary Fig. 8). Previous multi-patch-clamp studies have reported comparable subthreshold signals and attributed them to excitatory postsynaptic potentials in which a pre-synaptic cell triggers the firing of the postsynaptic cell[2,26]. This suggests that our U-NWFET devices can measure biologically relevant subthreshold signals and could be used for future studies of neural connections and synaptic activity.

After achieving neuronal intracellular recording, we asked whether the U-NWFET probes could be generalized to other electrogenic cells. To answer this, we cultured human induced pluripotent stem cell-derived cardiomyocytes (HiPSC-CMs) (see Methods). Contact of a HiPSC-CM and a U-NWFET probe of ~50 nm FET length and 0.75 μm ROC (Supplementary Fig. 9a,b) initially yielded a ~25 mV drop in the baseline, followed by periodic

~50 mV positive waveforms with a sharp rising phase (<50 ms), slow falling phase (~400 ms) and frequency of 1.25 ± 0.04 Hz. The second measurement of the same cell resulted again in a drop in the baseline potential and initial ~50 mV positive waveforms with frequencies of 1.23 ± 0.02 Hz (Supplementary Fig. 9c,d). Notably, the waveform frequency, amplitude and shapes during the first and second entry remain similar and are consistent with reported cardiac action potentials[27], suggesting that the U-NWFET probe is also able to record the intracellular potential of cardiac cells, and that the internalization process is minimally invasive.

Effect of nanowire geometry and sensor size on recording

We first investigated geometry effects by fabricating probe arrays with ROCs ranging from 0.75 to 2.0 μm (Fig. 4a and Supplementary Fig. 10) with fixed ~50 nm sensor sizes, carrying out ~30 measurements for each ROC from both DRG neurons and HiPSC-CMs.
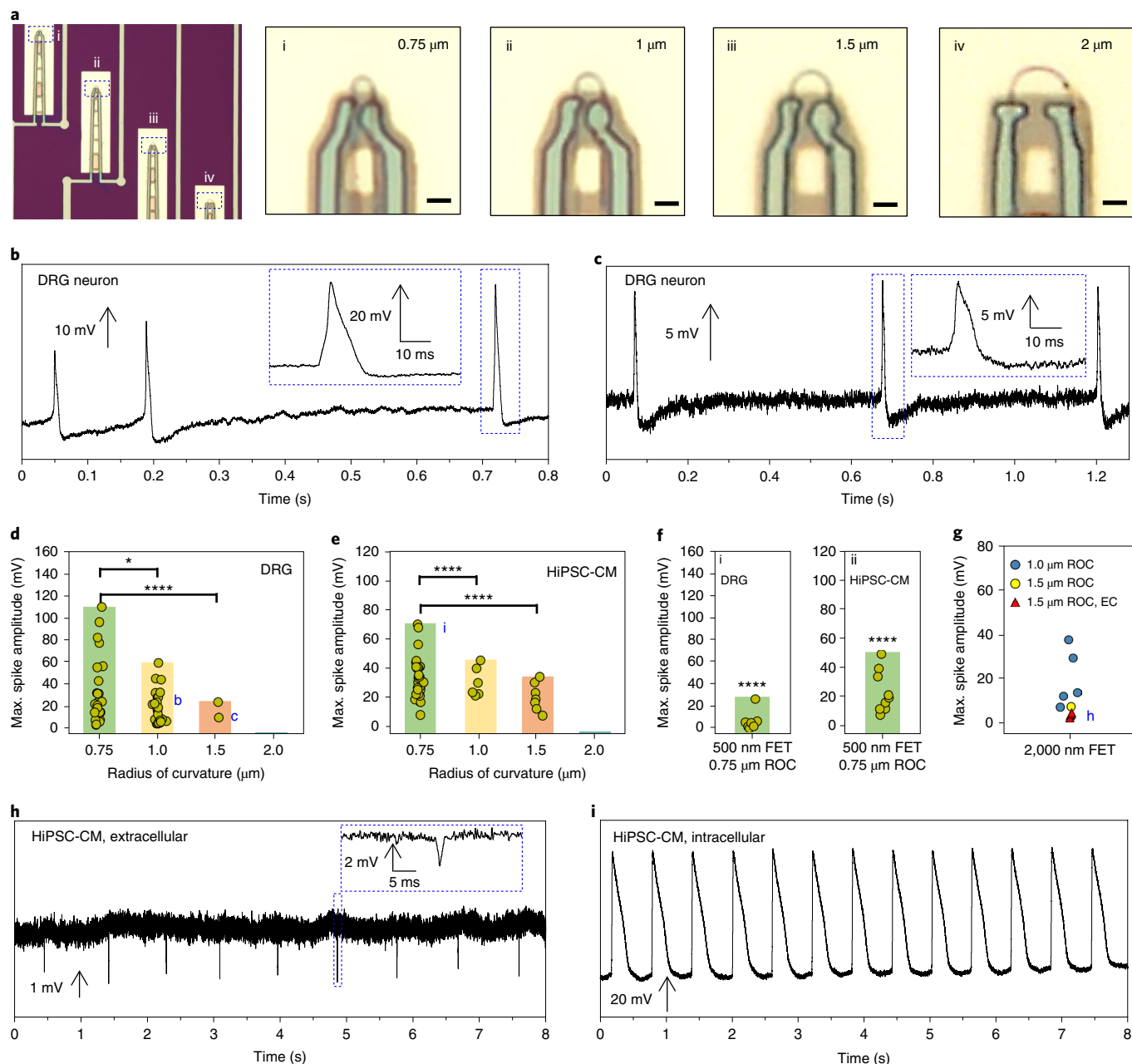
Fig. 4 | Effect of size and geometry of U-NWFET probes on electrophysiological recordings. a, Optical image of U-NWFET probes with different ROC before deposition of a Ni diffusion layer of 0.75 μm (i), 1 μm (ii), 1.5 μm (iii) and 2 μm (iv). Scale bars, 2 μm. **b,c**, Intracellular/intracellular-like recording from a DRG neuron by a ~50 nm FET channel length probe with 1 μm (**b**) and 1.5 μm (**c**) ROC. Insets, magnified views of selected action potentials. **d,e**, Plot of maximum recorded spike amplitude of recorded action potentials from DRG neurons (**d**) and HiPSC-CMs (**e**) versus ROC with fixed ~50 nm FET length. Coloured bars indicate the maximum spike amplitudes measured in the given dataset. The statistical significances were obtained by comparing the datasets below the ends of the black line using Student's *t*-test. *$P < 0.1$, ****$P < 0.0001$. The blue letters 'b', 'c' and 'i' highlight the data points from **b**, **c** and **i**. **f**, Scatter plot of maximum recorded spike amplitude of DRG neurons (i) and HiPSC-CMs (ii) for ~500 nm FET channel lengths with 0.75 μm ROC. The statistical significances **** shown in i and ii were obtained by comparing the datasets in i and ii with datasets of ROC 0.75 μm in **d** and **e**, respectively. **g**, Plot of maximum recorded spike amplitude of HiPSC-CMs with ~2,000 nm FET channel. Blue circles, intracellular data recorded from U-NWFETs with 1.0 μm ROC. Yellow circles, intracellular data recorded from U-NWFET with 1.5 μm ROC. Red triangles, extracellular (EC) data recorded from U-NWFETs with 1.5 μm ROC. Letter 'h' represents the data point for the trace shown in **h**. Note that for all scatter plots, ~30 measurements were attempted for each U-NWFET channel length and ROC, and recordings that did not result in measurement of intracellular/intracellular-like or extracellular action potentials were considered as 0 mV max spike amplitude and not shown for clarity but are summarized in Supplementary Table 3. **h**, Extracellular recording from HiPSC-CMs by an ~2,000 nm FET channel length probe with 1.5 μm ROC. Inset, magnified view of the highlighted spike. **i**, Intracellular recording from HiPSC-CMs by an ~50 nm FET channel length probe with 0.75 μm ROC.

For DRG neurons, representative intracellular/intracellular-like recordings were obtained by probes with 1 μm and 1.5 μm ROC (Fig. 4b,c), showing maximum action potential amplitudes of

~35 mV and ~12 mV, respectively. The distribution of maximum recording amplitudes from both cell types (Fig. 4d,e) shows the average values for DRG/HiPSC-CM cells and number of successful
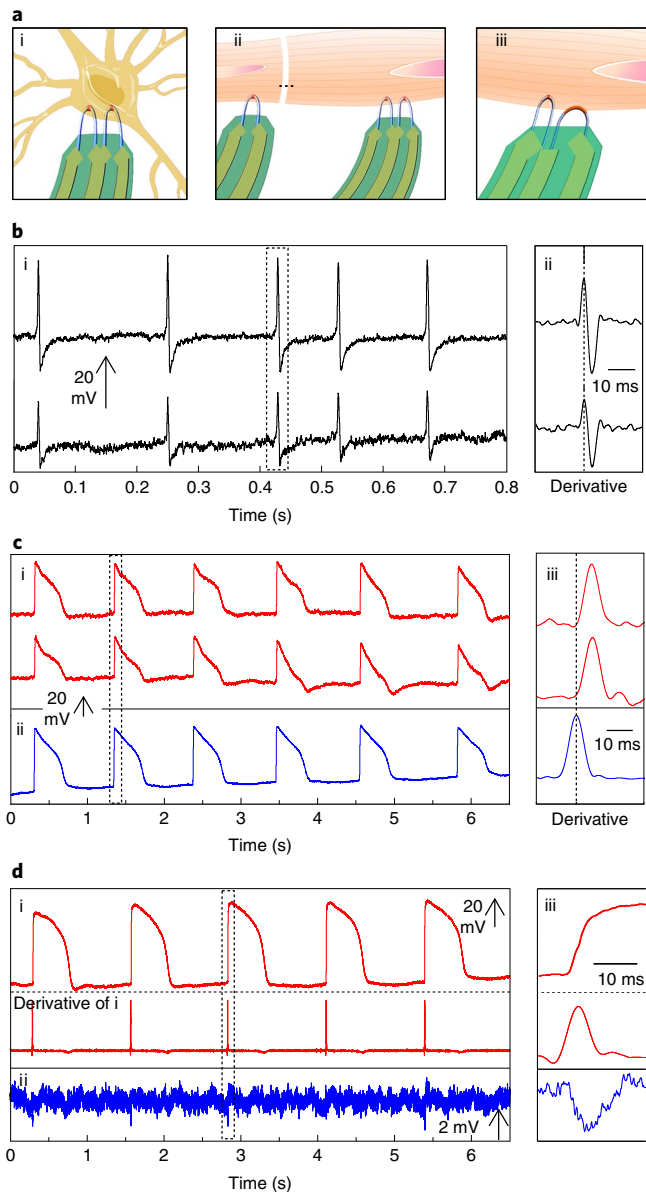
Fig. 5 | Multiplexed electrophysiological recording by U-NWFET probes.
a, Schematics of simultaneous multisite intracellular recording from a single neuron by paired U-NWFETs on one probe arm (i), multiplexed intracellular recording from different cells by U-NWFETs on different probe arms (ii) and simultaneous intracellular/extracellular recording from one cell by paired U-NWFETs on one probe arm (iii). **b**, Simultaneous intracellular recording from one DRG neuron by two ~50 nm FETs with 0.75 μm ROC on one probe arm with a 2 μm separation (i); derivative of traces in the region marked by a dashed box (ii). The vertical dashed guiding line in ii indicates the time point of the first action potential. No time delay is observed. **c**, Multiplexed intracellular recording from two HiPSC-CMs by one paired U-NWFET probe (i) and one single U-NWFET probe (ii); derivative of the marked region (iii). The two probes arms are fabricated with a distance of 350 μm between them. **d**, Simultaneous intracellular/extracellular recording from one HiPSC-CM by one ~50 nm FET with 0.75 μm ROC (top red trace, original intracellular signal; bottom red trace, derivative of intracellular signal) (i) and one ~2,000 nm FET with 1.5 μm ROC on one probe arm with a 2 μm separation (ii). (iii) Closer examination of the marked region.

recordings (out of ~30 measurements) of 34 ± 30 ($N = 24$)/34 ± 14 ($N = 31$), 19 ± 15 ($N = 25$)/31 ± 9 ($N = 6$) and 16 ± 7 ($N = 2$)/21 ± 9 ($N = 7$) mV for 0.75, 1.0 and 1.5 μm ROC, respectively. Interestingly,

the 2.0 μm ROC probes did not yield successful recordings on either cell type, indicating that increasing ROC correlates with lower recorded maximum amplitudes. Measurement of device transconductance (Supplementary Fig. 11) and SEM images (Supplementary Fig. 12) indicate that device characteristics do not change following measurement.

Second, we studied how sensor size affects recording by fabricating U-NWFETs with channel lengths of 500 nm and 0.75 μm ROC (Supplementary Fig. 10). Measurements made on both DRG neurons and HiPSC-CMs showed 8 ± 8 ($N = 7$) and 23 ± 13 mV ($N = 10$) maximum intracellular action potential amplitudes, respectively (Fig. 4f). Furthermore, U-NWFETs with channel lengths of ~2,000 nm and ROC of either 1.0 μm or 1.5 μm yielded maximum amplitudes of 21 ± 12 mV ($N = 5$, blue circles) and 8.0 mV ($N = 1$, yellow circle), respectively (Fig. 4g). Some of the 1.5 μm ROC, 2,000 nm channel U-NWFETs recorded negative spikes with maximum amplitudes of 4 ± 1 mV ($N = 4$, red triangles), while no successful recordings were achieved on DRG cells with 2,000 nm channel probes. A representative trace showing negative spikes from a HiPSC-CM (Fig. 4h) highlights their periodic negative short <3 ms duration that contrasts with a representative intracellular recording[27] obtained from a HiPSC-CM using a 0.75 μm ROC, 50 nm U-NWFET (Fig. 4i). The above data show that reducing the ROC and FET channel length has a statistically significant correlation with increases in both the maximum measured action potential amplitudes and number of successful recordings (Supplementary Table 3). At the most extreme limit, devices with 2 μm ROC no longer record action potentials, although devices with 1.5 μm ROC and 2,000 nm channel lengths recorded waveforms characteristic of extracellular signals[27,28]. We hypothesize that the observed increase in recording amplitude with decreasing ROC and channel length is not solely from physical interactions between the device and the cell but also a consequence of reported results demonstrating that nanoscale curvature can induce activation of endocytosis and related biological pathways[17–20,29]. Our studies indicate that using nanoscale topography to enhance device uptake is critical for developing tools that faithfully capture intracellular action potential features.

We also examined the relationship between U-NWFET device ROC and channel length and the intracellular recording duration. For both DRG neurons and HiPSC-CMs, there was no significant difference ($P > 0.05$) in recording duration with ROC (Supplementary Fig. 13 and Supplementary Table 4). Additionally, we observed that increasing the channel lengths showed no difference in recording duration in the DRG cells ($P > 0.05$), while for the HiPSC-CMs channel length increasing from 50 to 500 nm for the 0.75 μm ROC and from 50 to 2,000 nm for the 1.0 μm ROC U-NWFET resulted in a statistically significant ($P = 0.007$ and 0.027, respectively) increase in recording duration (Supplementary Fig. 13 and Supplementary Table 4). The lack of correlation between ROC and recording distribution suggests that loss of intracellular access is related to curvature-independent factors. We attribute the observed increase in recording duration for longer channel length measurements on HiPSC-CMs to the higher probability of maintaining a partially internalized configuration during cell contraction-induced instabilities. Recordings obtained on DRG neurons have shorter duration than HiPSC-CMs, possibly reflecting the reported differences in cell membrane mechanical properties as neuron membranes are generally less fluidic than those of cardiac cells[30].

We further ask whether deterministic fabrication with size and geometry control could enable multisite intracellular recording within a single cell using two U-NWFETs on one probe arm, recording from cell networks using independent U-NWFET probes, and/or simultaneous measurement of intracellular/extracellular action potentials from a single cell by two U-NWFETs with different ROC and channel lengths (Fig. 5a). First, a single DRG neuron soma was brought into contact with a pair of U-NWFETs

(each with an ~50 nm channel and 0.75 μm ROC) separated by 2 μm on one probe arm. The simultaneously recorded intracellular action potential amplitudes (Fig. 5b(i)) exhibited values of 46 and 28 mV from the two U-NWFETs. The derivative of two action potentials signals (Fig. 5b(ii)) and overlay of the two traces scaled to the same peak amplitudes (Supplementary Fig. 14a,b) shows that the peaks coincide with each other, indicating there is no discernible delay or waveform difference observed in the soma between the two channels.

Second, a layer of cultured HiPSC-CMs was brought into contact with paired U-NWFETs on the same probe arm (2 μm separation) and a third single U-NWFET probe separated by 350 μm from the paired probe (all three U-NWFETs with ~50 nm channel and 0.75 μm ROC). The paired probe recorded the intracellular action potential within one cell with action potential amplitudes of 54 mV and 47 mV (Fig. 5c(i)) in the two channels, while the third probe simultaneously recorded from another cell with an amplitude of 62 mV (Fig. 5c(ii)). Comparison of the time derivatives (Fig. 5c(iii)) showed no discernible delay in the paired channels, while there was ~6 ms delay between paired and single probes. This delay time and probe separation yield a signal propagation speed of ~5.8 cm s^{-1}, which agrees with that reported in the literature[31]. An overlay of the action potentials (Supplementary Fig. 14c,d) shows good agreement in the rising phase, and small deviations in the repolarization phase that can be attributed to different changes in the two U-NWFET/cell junctions as a result of mechanical contraction[32].

Third, paired U-NWFETs containing one ~50 nm FET with 0.75 μm ROC and one ~2,000 nm FET with 1.5 μm ROC on a single probe arm with 2 μm separation were fabricated and brought into contact with a HiPSC-CM (Fig. 5d). The channel with the ~0.75 μm ROC and 50 nm FET measured waveforms of ~50 mV characteristic of intracellular cardiac action potentials (Fig. 5d(i)), while the channel with the 2.0 μm ROC and ~2,000 nm FET measured sharp downward spikes of ~2 mV and <5 ms duration characteristic of extracellular cardiac action potentials (Fig. 5d(ii)). Close examination of the rising phase and derivative of the intracellular trace in comparison to the extracellular trace (Fig. 5d(iii)) shows that the measured extracellular signal is dominated by a downward peak at the same time as the upwards phase of the action potential. Extracellular waveforms measured using metal electrodes show increasing potential from capacitive coupling with the intracellular space, which should be aligned with the time derivative of the intracellular signal[28,33], followed by a decrease from the inward Na$^+$ current during action potential firing[33]. Our observed monophasic negative waveform suggests the small size of our recording element decreases capacitive coupling with the interior of the cell so that only local potential changes derived from inward Na$^+$ currents are observed. Furthermore, previous reports of simultaneous extracellular and intracellular measurement required separate patch-clamp and metal electrode array recording systems, which can introduce complications such as spatial mismatch of recording sites and difficulty in temporal synchronization[28,33]. In comparison, our multiplexed measurement strategy provides more localized information to correlate the extracellular and intracellular action potentials.

Finally, we demonstrate the scalability of our U-NWFET devices by fabricating six device regions containing 135 working single or multi U-NWFET devices (out of 168 addressable device sites) on a 76 mm wafer (Supplementary Fig. 15a,b). For typical cell experiments, the wafer is subsequently 'diced' to yield six chips that are individually mounted on printed circuit boards (Supplementary Fig. 5a). Separate measurements from HiPSC-CMs for each of the six chip device arrays yielded an intracellular signal from at least eight devices for each chip (Supplementary Fig. 15c). In one device array, we designed a series of probes containing 1–4 nanowires per probe arm (Supplementary Fig. 16a,b), and show simultaneous recording of action potentials in 10 channels from four separate

cells (Supplementary Fig. 16c). These experiments validate the potential for using our U-NWFET probes for multiplexed recording to study the electrophysiology of cell networks.

Conclusions

In summary, we have demonstrated that the scalable ultrasmall U-NWFET probe arrays fabricated using deterministic shape-controlled nanowire assembly and selective spatially defined solid-state semiconductor-to-metal transformation have the capability to record full amplitude intracellular action potentials from primary neurons and other electrogenic cells, and have the capacity for multiplexed recordings. These new studies complement other efforts from several groups focused on developing solid-state nanodevices for cell electrophysiology. Although our number of recording channels is limited compared to the hundreds of channels demonstrated in electrode-array-based strategies[12,14], it is notable that our U-NWFETs show the capability to record full amplitude intracellular actions potentials that are similar to patch-clamp recordings, but now in a scalable format. This flexible device structure/fabrication approach has further provided direct information about the relationship between recording amplitude as a function of device curvature and size, and thus supports the developing 'curvature hypothesis' relating nanotopography to endocytosis and cytoskeleton dynamics[17]. One key challenge, encountered both by U-NWFETs and other nanodevices, is the long-term stability of the intracellular recording. We hypothesize that future studies exploring either (1) chemical anchoring via surface functionalization with groups that can bind to the actin cytoskeletal localized near highly curved membranes[17,18,25] or (2) physical anchoring using spicule mesostructures[34] and/or modulation of nanowire morphology[29] to increase the physical detachment force could improve the stability of the intracellular device configuration. Supporting the potential of these proposed directions, previous experiments indicate that functionalized free-standing nanowires can remain in the interior of neurons for at least several hours[35]. More generally, this deterministic nanowire-based fabrication strategy can be incorporated into other platforms, such as free-standing probes[16], which allow precise targeting of individual cells or subcellular structures, and mesh electronics[36,37] for in vivo measurements.

Online content

Any methods, additional references, Nature Research reporting summaries, source data, statements of code and data availability and associated accession codes are available at https://doi.org/10.1038/s41565-019-0478-y.

References

1. Chen, R., Canales, A. & Anikeeva, P. Neural recording and modulation technologies. *Nat. Rev. Mater.* **2**, 16093 (2017).
2. Spira, M. E. & Hai, A. Multi-electrode array technologies for neuroscience and cardiology. *Nat. Nanotechnol.* **8**, 83–94 (2013).
3. Kruskal, P. B., Jiang, Z., Gao, T. & Lieber, C. M. Beyond the patch clamp: nanotechnologies for intracellular recording. *Neuron* **86**, 21–24 (2015).
4. Savtchenko, L. P., Poo, M. M. & Rusakov, D. A. Electrodiffusion phenomena in neuroscience: a neglected companion. *Nat. Rev. Neurosci.* **18**, 598 (2017).
5. Hamill, O. P., Marty, A., Neher, E., Sakmann, B. & Sigworth, F. J. Improved patch-clamp techniques for high-resolution current recording from cells and cell-free membrane patches. *Pflugers Arch.* **391**, 85–100 (1981).
6. Martina, M. & Taverna, S. *Patch-clamp Methods and Protocols*, 2nd edn (Humana Press, 2014).
7. Jiang, Y. W. et al. Rational design of silicon structures for optically controlled multiscale biointerfaces. *Nat. Biomed. Eng.* **2**, 508–521 (2018).
8. Parameswaran, R. et al. Photoelectrochemical modulation of neuronal activity with free-standing coaxial silicon nanowires. *Nat. Nanotechnol.* **13**, 260–266 (2018).

9. Abbott, J., Ye, T. Y., Ham, D. & Park, H. Optimizing nanoelectrode arrays for scalable intracellular electrophysiology. *Acc. Chem. Res.* **51**, 600–608 (2018).
10. McGuire, A. F., Santoro, F. & Cui, B. X. Interfacing cells with vertical nanoscale devices: applications and characterization. *Annu. Rev. Anal. Chem.* **11**, 101–126 (2018).
11. Spira, M. E., Shmoel, N., Huang, S. H. M. & Erez, H. Multisite attenuated intracellular recordings by extracellular multielectrode arrays, a perspective. *Front. Neurosci.* **12**, 212 (2018).
12. Abbott, J. et al. CMOS nanoelectrode array for all-electrical intracellular electrophysiological imaging. *Nat. Nanotechnol.* **12**, 460–466 (2017).
13. Dipalo, M. et al. Intracellular and extracellular recording of spontaneous action potentials in mammalian neurons and cardiac cells with 3D plasmonic nanoelectrodes. *Nano Lett.* **17**, 3932–3939 (2017).
14. Dipalo, M. et al. Plasmonic meta-electrodes allow intracellular recordings at network level on high-density CMOS-multi-electrode arrays. *Nat. Nanotechnol.* **13**, 965–972 (2018).
15. Tian, B. Z. et al. Three-dimensional, flexible nanoscale field-effect transistors as localized bioprobes. *Science* **329**, 830–834 (2010).
16. Qing, Q. et al. Free-standing kinked nanowire transistor probes for targeted intracellular recording in three dimensions. *Nat. Nanotechnol.* **9**, 142–147 (2014).
17. Lou, H. Y., Zhao, W. T., Zeng, Y. P. & Cui, B. X. The role of membrane curvature in nanoscale topography-induced intracellular signaling. *Acc. Chem. Res.* **51**, 1046–1053 (2018).
18. Zhao, W. T. et al. Nanoscale manipulation of membrane curvature for probing endocytosis in live cells. *Nat. Nanotechnol.* **12**, 750–756 (2017).
19. Iversen, L., Mathiasen, S., Larsen, J. B. & Stamou, D. Membrane curvature bends the laws of physics and chemistry. *Nat. Chem. Biol.* **11**, 822–825 (2015).
20. Kaksonen, M. & Roux, A. Mechanisms of clathrin-mediated endocytosis. *Nat. Rev. Mol. Cell Biol.* **19**, 313–326 (2018).
21. Zhao, Y. et al. Shape-controlled deterministic assembly of nanowires. *Nano Lett.* **16**, 2644–2650 (2016).
22. Wu, Y., Xiang, J., Yang, C., Lu, W. & Lieber, C. M. Single-crystal metallic nanowires and metal/semiconductor nanowire heterostructures. *Nature* **430**, 61–65 (2004).
23. Study, R. E. & Kral, M. G. Spontaneous action potential activity in isolated dorsal root ganglion neurons from rats with a painful neuropathy. *Pain* **65**, 235–242 (1996).
24. Delmas, P., Hao, J. & Rodat-Despoix, L. Molecular mechanisms of mechanotransduction in mammalian sensory neurons. *Nat. Rev. Neurosci.* **12**, 139–153 (2011).
25. Aalipour, A., Xu, A. M., Leal-Ortiz, S., Garner, C. C. & Melosh, N. A. Plasma membrane and actin cytoskeleton as synergistic barriers to nanowire cell penetration. *Langmuir* **30**, 12362–12367 (2014).
26. Cossell, L. et al. Functional organization of excitatory synaptic strength in primary visual cortex. *Nature* **518**, 399–403 (2015).
27. Burridge, P. W. et al. Chemically defined generation of human cardiomyocytes. *Nat. Methods* **11**, 855–860 (2014).
28. Sanders, K. M., Ward, S. M. & Hennig, G. W. Problems with extracellular recording of electrical activity in gastrointestinal muscle. *Nat. Rev. Gastroenterol. Hepatol.* **13**, 731–741 (2016).
29. Dipalo, M. et al. Cells adhering to 3D vertical nanostructures: cell membrane reshaping without stable internalization. *Nano Lett.* **18**, 6100–6105 (2018).
30. Dietschy, J. M. & Turley, S. D. Thematic review series: brain lipids. Cholesterol metabolism in the central nervous system during early development and in the mature animal. *J. Lipid Res.* **45**, 1375–1397 (2004).
31. Zhu, H. Q. et al. Two dimensional electrophysiological characterization of human pluripotent stem cell-derived cardiomyocyte system. *Sci. Rep.* **7**, 43210 (2017).
32. Woodcock, E. A. & Matkovich, S. J. Cardiomyocytes structure, function and associated pathologies. *Int. J. Biochem. Cell Biol.* **37**, 1746–1751 (2005).
33. Gold, C., Henze, D. A., Koch, C. & Buzsáki, G. On the origin of the extracellular action potential waveform: a modeling study. *J. Neurophysiol.* **95**, 3113–3128 (2006).
34. Luo, Z. et al. Atomic gold—enabled three-dimensional lithography for silicon mesostructures. *Science* **348**, 1451–1455 (2015).
35. Lee, J. H., Zhang, A. Q., You, S. S. & Lieber, C. M. Spontaneous internalization of cell penetrating peptide-modified nanowires into primary neurons. *Nano Lett.* **16**, 1509–1513 (2016).
36. Fu, T. M. et al. Stable long-term chronic brain mapping at the single-neuron level. *Nat. Methods* **13**, 875–882 (2016).
37. Hong, G. S. et al. A method for single-neuron chronic recording from the retina in awake mice. *Science* **360**, 1447–1451 (2018).

Author contributions

Y.Z., S.S.Y. and C.M.L. conceived and designed the experiments. Y.Z., S.S.Y. and A.Z. performed the experiments and analysed the data. Y.Z., S.S.Y., A.Z. and C.M.L. co-wrote the paper. All authors discussed the results and commented on the manuscript.

Competing interests

The authors declare no competing interests.

Additional information

Supplementary information is available for this paper at https://doi.org/10.1038/s41565-019-0478-y.

Reprints and permissions information is available at www.nature.com/reprints.

Correspondence and requests for materials should be addressed to C.M.L.

Journal peer review information: *Nature Nanotechnology* thanks Bozhi Tian, Bruce Wheeler and other anonymous reviewer(s) for their contribution to the peer review of this work.

Publisher's note: Springer Nature remains neutral with regard to jurisdictional claims in published maps and institutional affiliations.

Methods

Nanowire synthesis. Si nanowires (p-type, 15 nm diameter) were synthesized using a gold nanocluster-catalysed vapour–liquid–solid growth method[21]. Growth substrates (15 × 60 mm² pieces of Si wafer with 600 nm thermal oxide, Nova Electronic Materials) were oxygen plasma cleaned (100 W, 2 min, 50 cubic centimetres per minute (s.c.c.m.) O₂, PJ Plasma Surface Treatment System), treated with poly-L-lysine solution (0.1%, 150,000–300,000 g mol⁻¹, Ted Pella) for 5 min, rinsed thoroughly with deionized (DI) water and dried with nitrogen. Then, 1 ml of aqueous solution of 10 nm gold nanoparticles (Ted Pella) with a concentration of 1.9×10^{12} particles per ml was dispersed[38] on the substrate for 2 min followed by thorough rinsing with DI water and drying with nitrogen (gold nanoparticle surface concentration, 0.01–0.04 particles per μm²). The substrate was then placed into a home-built chemical vapour deposition reactor and the system was evacuated to a base pressure of 0.6 mtorr. Nanowires were synthesized at 430 °C at a total pressure of 40 torr with gas flow rates of 2.5 s.c.c.m. silane (SiH₄, 99.9999%, Voltaix) as the silicon reactant, 3.1 s.c.c.m. diborane (B₂H₆, 100 ppm in H₂, Voltaix) as the p-type dopant, and 60 s.c.c.m. hydrogen (H₂, 99.999%, Matheson) as the carrier gas. Typical growth times of 1 h yielded nanowires with average lengths of ~50 μm.

U-NWFET probe array fabrication. Key steps involved in the fabrication of U-NWFET probe arrays are shown in Fig. 2 and Supplementary Fig. 1, with the key parameters as follows:

(1) LOR 3A (Microchem) and diluted S1805 (S1805: Thinner-P = 1:2 (vol:vol), Microchem) were spin-coated on a Si₃N₄/SiO₂-coated Si wafer (200 nm Si₃N₄, 100 nm SiO₂ on p-type Si, 0.005 Ω cm, or 600 nm thermal SiO₂ on n-type Si, 0.005 Ω cm, Nova Electronic Materials) and baked at 180 °C for 5 min and at 115 °C for 1 min, respectively. The photoresist was patterned by photolithography with a Maskless aligner (MLA150) and developed (MF-CD-26, MicroChem Corp.) for 30 s. Following this photolithography process, a 60-nm-thick Ni sacrificial layer was deposited by thermal evaporation (Sharon Vacuum Co.), followed by a liftoff step (Remover PG, MicroChem Corp.) (Supplementary Fig. 1a). The size of the Ni sacrificial layer was designed to accommodate the size of the U-NWFET probe: 30 μm × 100 μm for single U-NWFET probes (Supplementary Fig. 1h(i)) or 90 μm × 100 μm for up to four U-NWFETs probes per bend-up probe arm (Supplementary Fig. 1h(ii)).

(2) The photolithography process in step 1 was repeated to define an 80-μm-long bottom region for sputter deposition of a 60 nm Si₃N₄ passivation layer (Orion 3 Sputtering Systems, AJA International). The main body of the Si₃N₄ passivation layer (75 μm long) was deposited on the Ni sacrificial layer with 5 μm Si₃N₄ extending outside of the sacrificial region (Supplementary Fig. 1b).

(3) LOR 1A (Microchem) and diluted S1805 (S1805: Thinner-P = 1:2 (vol:vol)) were spin-coated and baked at 180 °C for 5 min and at 115 °C for 1 min, respectively. The photolithography process in step 1 was repeated to define arrays of trenches with shapes and ROCs as described in the main text (Supplementary Fig. 1c).

(4) The shape-controlled deterministic nanowire assembly was used to align disordered straight nanowires into U-shaped arrays as described previously[21] (Supplementary Fig. 1d). Briefly, a wafer with an array of trenches was mounted onto a micromanipulator-controlled movable stage, covered with mineral oil (viscosity $\nu \approx 70$ mPa s, #330760, Sigma-Aldrich) as the lubricant, and then the nanowire growth substrate was brought into contact with the target substrate with controlled contact pressure. The target substrate was moved at a constant velocity of ~5 mm min⁻¹ with respect to the fixed nanowire growth substrate; the growth substrate was then removed and the target substrate rinsed with octane (98%, Sigma-Aldrich) to remove the lubricant. Estimations of the U-shaped nanowire strain were calculated and are shown in Supplementary Table 2.

(5) Al₂O₃ was deposited directly after the nanowire assembly by atomic layer deposition (S200, Cambridge NanoTech) with 1 cycle (1.4 Å) at 80 °C to fix the U-shaped nanowires on the bottom passivation layer and then all photoresist was removed in Remover PG (Supplementary Fig. 1e).

(6) Step 1 was repeated to simultaneously pattern electrical interconnects to the U-NWFET as well as connects to the large pads used as the input/output (I/O) region. Native oxide on the nanowire was etched with a buffered oxide etch (BOE, 7:1, Microchem) for 10 s before thermal deposition of asymmetrically strained metal Cr/Au/Cr (1.5/60/60 nm). The strained metal leads the U-NWFET probe to bend off the wafer surface following etching of the sacrificial layer, like that described in previous work[21].

(7) Step 2 was repeated to deposit 60 nm of Si₃N₄ as electrical passivation over exposed metal features except for the I/O pad region (Fig. 2b and Supplementary Fig. 1f).

(8) Electron-beam lithography (EBL) or photolithography was used to define the Ni diffusion region with shape and position as described in the main text. Specifically, EBL was used for U-NWFET probes with ~50 nm (Fig. 2c) and ~500 nm (Supplementary Fig. 2c) channel length. For the EBL process, copolymer MMA (EL6, Microchem) and polymethyl methacrylate (PMMA, 950-C2, Microchem) were spin-coated and baked at 180 °C for 5 min, sequentially. The resists were then patterned with an EBL system (ELS-F125,

Elionix) and developed (MIBK/IPA 1:1, MicroChem Corp.) for 60 s. For U-NWFET probe with ~2,000 nm channel length (Supplementary Fig. 2d), the same photolithography process in step 1 could be used to define regions for Ni deposition. Native oxide on the nanowire was removed by BOE for 10 s before deposition of 20 nm Ni via thermal evaporation. After liftoff, the chip was annealed using a Rapid Thermal Processor (RTP, 600xp, Modular Process Technology) in forming gas (H₂:N₂ 10:90) at 350 °C for 5 min to transform the Si nanowire segments underneath and adjacent to the Ni diffusion layer to nickel silicide[22], thereby generating a localized sensing element (Supplementary Fig. 1g).

(9) Polydimethylsiloxane (PDMS) was prepared by first pouring Sylgard 184 (Dow Corning) elastomer (mixed in a 10:1 ratio of base to curing agent) into a Petri dish, and then curing overnight at 55 °C in a convection oven. A PDMS chamber with ~20 × 30 mm² opening and ~0.5 cm sidewalls was cut from the cured PDMS and mounted around the device region using Kwik-Sil silicone adhesive (World Precision Instruments). A printed circuit board (PCB, UXCell) connector was then mounted adjacent to the I/O region of the devices and wire-bonded to the U-NWFET probe I/O pads (Supplementary Fig. 5a). Probes were kept in a Dry-Keeper desiccator cabinet (H-B Instrument-Bel-Art). Before electrical characterizations and/or electrophysiological measurements, the Ni sacrificial layers and remaining Ni from the diffusion layer were removed in nickel etchant (Nickel Etchant TFB, Transense) for 3–5 min, which allowed release of these devices into a 3D bend-up structure (Fig. 2d and Supplementary Fig. 1h). Following release, the devices were rinsed in DI water 5–10 times for 20 s each.

Device characterization. Overview optical images of the measurement set-up and U-NWFET probe chip to instrument I/O area were acquired with an SLR digital camera (Canon), and higher-resolution bright-field optical images of individual U-NWFET probes and probe arrays were acquired by an Olympus BX50WI system with Andor Luca electron-multiplying charge-coupled device camera. High-resolution SEM images of nanowires, including intermediate fabrication steps, were acquired using a Zeiss Ultra Plus field emission SEM (Carl Zeiss). A BSE detector was used to obtain high-resolution composition-sensitive maps based on the electron elastic scattering difference of atomic number on the sample. U-NWFETs fabricated for characterization did not have a Ni sacrificial layer to improve contrast during SEM imaging. The BSE images show the silicon and nickel silicide segments on U-shaped nanowires: the bright region indicates nickel/nickel silicide and the dark region indicates p-type Si.

For electrical characterization, one arm of the U-NWFET was considered as the source, and the other arm is considered as the drain. Voltage V_{ds} was applied between the source and drain of the U-NWFET, and the resulting current, I_{ds}, was measured. The electrical conductance (I_{ds}/V_{ds}) of the U-NWFET devices was measured in the dry state by sweeping V_{ds} between −1 and 1 V and measuring I_{ds} using a homemade battery-powered 16-channel current preamplifier with bandwidth of 6 kHz, which amplified the current signal for recording using a 16-channel analog-to-digital converter (Axon Digidata 1440A, Molecular Devices) controlled by pCLAMP 10.7 software (Molecular Devices). The $I_{ds}–V_{ds}$ data were recorded in an air/dry state.

Surface functionalization of U-NWFET probes. Phospholipid vesicles were prepared for use in functionalized U-NWFET probes in the following manner, similar to previous papers[15,16]. (1) 1,2-dimyristoyl-*sn*-glycero-3-phosphocholine (DMPC, Avanti Polar Lipids) was suspended in chloroform (anhydrous, >99%, Sigma-Aldrich) to a concentration of 20 mg ml⁻¹ and mixed with 1% mass of 1-myristoyl-2-[12-[(7-nitro-2-1,3-benzoxadiazol-4-yl)amino]dodecanoyl]-*sn*-glycero-3-phosphocholine (NBD-lipid, Avanti Polar Lipids). (2) The solution of DMPC/NBD-lipid was placed into a vacuum desiccator for at least 6 h to evaporate off the chloroform. (3) The resulting powder was resuspended in phosphate buffered saline (1× PBS, HyClone) to a concentration of 1 mg ml⁻¹ and the lipid solution was placed in a water bath at 37 °C for at least 2 h with periodic agitation using a vortex mixer (30 s every 20 min, Maxi Mix II, Barnstead/Thermolyne Corp.) to ensure full rehydration. (4) The resulting lipid solution was sonicated using a tip sonicator (25% amplitude, 10 s/15 s pulse on/off, Branson Ultrasonics Sonifier S-450l, Branson Ultrasonics) at ~37 °C for 2 h. (5) Following sonication, the lipid solution was sterile filtered (0.2 μm Acrodisc syringe filter, PN 4192, Pall Corp.) and used within 1 h of preparation.

Immediately before measurements, U-NWFET probe arrays with a mounted PDMS chamber (Supplementary Fig. 5b) were incubated for 2 h in 1.5 ml of the prepared lipid vesicle solution to allow functionalization of U-NWFET as reported previously for other nanowire devices[15,16]. Following incubation, the U-NWFET probe arrays were then rinsed in Tyrode's solution (in mM: NaCl 155, KCl 3.5, MgCl₂ 1, CaCl₂ 1.5, HEPES 10, D-glucose 10, pH 7.4 for DRG neurons, or NaCl 138, KCl 4, CaCl₂ 2, MgCl₂ 1, Na₂HPO₄ 0.33, HEPES 10, glucose 10, pH 7.4 for HiPSC-CMs, all chemicals in Tyrode's solution were purchased from Sigma-Aldrich) 5–10 times for 20 s, ~3 ml each.

Device characterization in Tyrode's solution. Following phospholipid modification, electrical measurements were carried out in Tyrode's solution.

The electrical conductance of the U-NWFETs was continuously measured by recording the drain–source current (I_{ds}) at a fixed source–drain d.c. bias between 0.1 and 0.2 V by the electronic measurement set-up mentioned above. The sensitivities (transconductance) were then obtained by sweeping an Ag/AgCl reference electrode (2.0 × 4.0 mm, E-201, Warner Instruments) between −100 mV and 100 mV and measuring the corresponding linear change in U-NWFET conductance. The measured average (in 10 samples) conductance of U-NWFETs for channel lengths of ~50 nm, ~500 nm and ~2,000 nm are 3.3 ± 0.6, 0.7 ± 0.2 and 0.3 ± 0.1 μS, with average sensitivities of 5.4 ± 1.3, 2.3 ± 0.7 and 0.9 ± 0.3 μS V⁻¹ respectively. An inverse relationship exists between conductance, and consequently transconductance, and channel length, as expected from the relationship: ($G = \sigma A/L$), where G is the channel conductance, σ is the electrical conductivity, A is the cross-sectional area of the wire and L is the channel length[39].

To estimate the noise level of the U-NWFETs devices, the conductance of the 10 devices for each channel length was measured using the Ag/AgCl reference electrode to fix the solution voltage at 0 for ~5 s. The standard deviation of the measured conductance was used to obtain the noise for each device in μS. Then, the transconductance of each device was used to convert the measured noise in μS into a value in mV, and the resulting number was multiplied by 3 to estimate the limit of detection as per convention. Averaging the 10 values for the limit of detection (in mV) for each channel length resulted in noise levels of 0.90 ± 0.60, 1.2 ± 0.9 and 1.9 ± 0.9 mV for the ~50, 500 and 2,000 nm devices, respectively.

Preparation of flexible cell culture substrates. A master mould for the culture substrate was first prepared by spin-coating SU-8 2000.5 (Microchem) onto a Si wafer and patterning repeating 3-μm-wide lines with 3 μm spacing using photolithography. After patterning, the master mould was hard baked on a hot plate at 180 °C for 2 h, and then silanized with tridecafluoro-1,1,2,2-tetrahydrooctyl-1-trichlorosilane (Sigma-Aldrich) for 2 h in a vacuum desiccator, to enhance release of the PDMS template from the master mould[40].

Flexible PDMS cell culture substrates were prepared by spin-coating Sylgard 184 elastomer mixed in a 10:1 ratio of base to curing agent onto the master mould at 250 r.p.m. for 1 min. The PDMS on the master mould was then cured in a convection oven set to 180 °C for 2 h, resulting in a thickness of ~220 μm, and cut into pieces (~10 × 10 mm²) for cell culture. Before cell culture, the PDMS substrates were autoclaved at 125 °C for 1 h, treated by O₂ plasma (100 W, 2 min, 50 s.c.c.m. O₂) and then washed in a 75% (vol/vol) solution of ethanol (200 proof, KOPTEC)/water for 1 h.

For DRG neuron culture, the PDMS was first functionalized with 40 μg ml⁻¹ poly-D-lysine (molecular weight of >300,000 g mol⁻¹, Sigma-Aldrich) in DI water for 1 h at room temperature. After poly-D-lysine functionalization, the PDMS was washed twice in DI water for 30 s each and air dried, and then functionalized with 20 μg ml⁻¹ laminin (Thermo Fisher Scientific) in Leibovitz's L-15 (Thermo Fisher Scientific) for 1 h at room temperature. Laminin solution was removed immediately before the cell suspension was plated on the PDMS.

For HiPSC-CM culture, the PDMS was functionalized sequentially with (1) 1% (3-aminopropyl)triethoxysilane (Sigma-Aldrich) in a 95% (vol/vol) solution of ethanol/DI water for 20 min at room temperature, followed by washing three times in ethanol for 30 s each, and three times in DI water for 30 s each; (2) 2.5% (vol/vol) glutaraldehyde (grade I, 50% in H₂O, Sigma-Aldrich)/water for 1 h at room temperature, followed by washing three times in DI water for 30 s each; (3) Geltrex matrix (Thermo Fisher Scientific) at 37 °C for ~8 h. The Geltrex solution was removed immediately before the cell suspension was plated onto the PDMS.

Cell culture. Dissociated DRG cells were prepared as described previously[35] and cultured in the CO₂ incubator overnight before use. Cells that can spontaneously fire (Supplementary Fig. 8) were selected for recording. HiPSC-CMs were cultured as described in the NCardia online protocol[41]. Cryogenically frozen Cor.4U HiPSC-CM vials (Cor.4U > 250k cells, Ncardia Group) were thawed in a 37 °C water bath, and 0.5 ml of proprietary Cor.4U cell medium (Ncardia Group) preheated to 37 °C was added to the vial. The cell solution was then homogenized by gentle aspiration and seeded at 75,000 cells per cm² to achieve confluency onto the prepared PDMS substrates. Immediately following cell seeding, the cell culture was left at room temperature for 20 min to allow the solution to settle and ensure an even distribution of cells. The cells were then cultured in a 5% CO₂, 37 °C incubator and the Cor.4U cell medium was changed 6 h following plating. Subsequently, the medium was changed every day and the cells were used within 2 weeks following seeding, once a uniformly contracting layer was observed.

Electrophysiological recording with U-NWFET. The Ag/AgCl reference electrode was used to fix the extracellular Tyrode's solution voltage to 0 V for cell measurements. A PDMS sheet with cultured DRG neurons or HiPSC-CMs was fixed upside down onto a homebuilt vacuum wand mounted on a 40 nm step resolution x–y–z micromanipulator (MP-285, Shutter Instruments) connected to a micromanipulator controller (MPC-200/ROE-200, Sutter Instruments) to position the cells over and bring the cells into contact with the U-NWFETs (Supplementary Fig. 5c). The Tyrode's solution was maintained at room temperature for the DRG neuron experiments and at ~37 °C for the HiPSC-CM experiments. For longer (>3 min) HiPSC-CM intracellular recording (Supplementary Fig. 9b,d), high pass filters were set to 0.4 Hz, similar to the approach used by other groups[12,42,43].

Patch-clamp recording. Patch-clamp recording was performed at room temperature using a Multiclamp 700B amplifier (Molecular Devices) and a Digidata 1440A Digitizer Acquisition System, controlled by pCLAMP 10.7 software (Molecular Devices). Micropipettes were prepared using a micropipette puller (P-97, Sutter Instruments) and the pipette tip resistance ranged between 5 and 10 MΩ. DRG neurons were cultured on a glass coverslip with the same modification as PDMS. Recording from DRG neurons was carried out in Tyrode's solution. The micropipettes were filled with an internal solution consisting of (in mM): potassium L-aspartate 140, NaCl 13.5, MgCl₂ 1.8, ethylene glycol-bis(2-aminoethylether)-N,N,N',N'-tetraacetic acid (EGTA) 0.09, HEPES 9, phosphocreatine di(tris) salt 14, adenosine 5′-triphosphate (ATP) magnesium salt 4, guanosine 5′-triphosphate (GTP) tris buffered 0.3, pH 7.2 adjusted with KOH[6]. All chemicals in the internal solution were purchased from Sigma-Aldrich, except GTP tris buffer, which was purchased from Thermo Fisher.

Data availability

The data that support the findings of this study are available from the corresponding author upon reasonable request.

References

38. Patolsky, F., Zheng, G. & Lieber, C. M. Fabrication of silicon nanowire devices for ultrasensitive, label-free, real-time detection of biological and chemical species. *Nat. Protoc.* **1**, 1711–1724 (2006).
39. Kittel, C. *Introduction to Solid State Physics* 8th edn (Wiley, 2005).
40. Minteer, S. D. *Microfluidic Techniques: Reviews and Protocols* (Humana Press, 2006).
41. *Cardiomyocytes User Manual* (NCardia, 2018); https://ncardia.com/files/documents/manuals/PluricyteCardiomyocyte_Manual_v2.pdf.
42. Shmoel, N. et al. Multisite electrophysiological recordings by self-assembled loose-patch-like junctions between cultured hippocampal neurons and mushroom-shaped microelectrodes. *Sci. Rep.* **6**, 27110 (2016).
43. Xie, C., Lin, Z., Hanson, L., Cui, Y. & Cui, B. Intracellular recording of action potentials by nanopillar electroporation. *Nat. Nanotechnol.* **7**, 185–190 (2012).